

Article

Optimization of Friction Stir Process Parameters for Enhancement in Surface Properties of Al 7075-SiC/Gr Hybrid Surface Composites

Namdev Ashok Patil ^{1,*}, Srinivasa Rao Pedapati ¹, Othman Bin Mamat ¹ and Abdul Munir Hidayat Syah Lubis ²

¹ Mechanical Engineering Department, Universiti Teknologi Petronas, Seri Iskandar, Perak 32610, Malaysia; srinivasa.pedapati@utp.edu.my (S.R.P.); drothman_mamat@utp.edu.my (O.B.M.)

² Department of Mechanical Engineering Technology, Universiti Teknikal Malaysia, Melaka 76100, Malaysia; munir@utem.edu.my

* Correspondence: namdev_17003401@utp.edu.my; Tel.: +60-149367158

Received: 5 November 2019; Accepted: 2 December 2019; Published: 6 December 2019



Abstract: Friction stir processing (FSP) has evolved as an important technique in fabrication of metal matrix composites. The surface properties enhancement is obtainable by insertion of desired discontinuous particular reinforcements into base alloy using FSP. Despite having high specific strength, more applications of Al alloys are restricted due to their poor surface properties under various loading conditions. In this study, the main focus is on enhancing the microhardness and wear properties of Al 7075 base alloy by means of uniform dispersion of silicon carbide and graphite (SiC/Gr) nano particles into the base alloy using the FSP technique. The tool rotational speed (w : 500, 1000, 1500 rpm), tool traverse speed (v : 20, 30, 40 mm/min), reinforcement particles hybrid ratio (HR: 60:40, 75:25, 90:10) and volume percentage (vol%: 4%, 8%, 12%) are used as independent parameters. The effect of these parameters on microstructure, micro hardness and wear properties of surface composites are studied in detail. For desired wear rate and microhardness as responses, the aforementioned independent parameters are optimized using response surface methodology (RSM). The significance of factors and their interactions for maximizing hardness and minimizing wear rate and coefficient of friction (COF) were determined. Analysis of variance (ANOVA) for responses has been carried out, and the models were found to be significant in all three responses. The minimum wear rate of 0.01194 mg/m was obtained for parameters w 1500 rpm, v 40 mm/min, HR 60:40, vol% 4 (Run 10). The maximum micro hardness of 300 HV obtained for parameters w 1000 rpm, v 30 mm/min, HR 75:25, vol% 12 (Run 14). The presence and uniform distribution of SiC and Gr into the base alloy was confirmed through field-emission scanning electron microscopy (FESEM) imaging, energy-dispersive X-ray spectroscopy (EDX) and mapping tests. The wear rate and COF decreased significantly due to graphitized mechanically mixed layer developed at the sliding contacts. The microhardness of resultant composites observed to be dependent on effect of the independent parameters on extent of inherent precipitates dissolution and grain size strengthening in the resultant materials.

Keywords: friction stir processing; hybrid surface composites; microstructure; response surface methodology; wear properties

1. Introduction

In the engineering materials field, the fabrication of composite materials, related design and manufacturing technology is a significant advance in the area of engineering materials. Many advanced

engineering applications require materials with a wide range of properties that are difficult to meet using monolithic material structures [1]. It has been noted that metal matrix composites (MMCs) offer such tailor-made property combinations required in a wide range of engineering applications [2]. In particular, composites have enhanced significant tribological properties to meet the needs of the important surface engineering field. With the reinforcement of ceramics particles, the surface properties of the material are improved significantly. The large application of composites to the aerospace, automotive, defense industry, etc. has influenced new researchers in the development and design of manufacturing techniques [3,4]. Recently, in surface engineering the surface metal matrix composites are also being fabricated through various methods like plasma spraying [5], cold spraying [6], laser melting [7–10], cast sinter [11,12], etc. Also the bulk metal matrix composites are produced by using the conventional methods like stir casting [13], powder metallurgy [14], mechanical alloying [15], etc. These fabrication techniques have many disadvantages such as reinforcement agglomeration, formation of detrimental phases, and interfacial reactions due to processing above melting point temperature [16,17]. Thus to overcome these disadvantages the researchers look for the other novel techniques. The friction stir-processing (FSP) technique overcomes many disadvantages due to processing below the melting point temperature of base alloys. Initially, R.S. Mishra et al. proposed FSP technique and have fabricated the Al-silicon carbide (SiC) ex-situ surface composites [18]. Then this solid state and eco-friendly technique became more popular among researchers and led to numerous research works on surface composites fabrication using FSP.

Aluminium alloys are replacing steel alloys in various applications due to their high specific strength and low density [19–21]. However, Weak surface properties, such as wear resistance under high-load conditions, limit their broader applications. Like steels, Al alloys cannot be greatly hardened by hardening induction due to the lack of martensitic phase [22]. The production of MMCs based on aluminium (Al) involves strengthening aluminium alloys with different particles to induce certain specific properties and improve some of their inherent limitations. The hybrid reinforcement approach gives space in MMCs for possible cost reduction along with multiple property optimization together. Many researchers reported comparable or enhanced performance for hybrid MMCs over single reinforcement MMCs even at lower processing costs. This puts hybrid reinforced composites under the spotlight as many investigators predict the enormous promise of producing high-performance and low-cost MMCs through this route [23].

Many authors reported a hybrid composite fabrication approach effective in enhancing broad spectrum of material properties. The mechanical properties of pure aluminium increased substantially by reinforcing multi-layer graphene [24] and SiC with graphene oxide nano sheets [25] through a FSP ex-situ approach. Dixit et al. [24] have developed the pure Al-graphene nano composites with exfoliation of graphite to graphene successfully using multi-pass FSP (8 passes). Sharma et al. [26] improved mechanical and corrosion properties of Al 6061 alloy by reinforcing a hybrid SiC/Gr combination. They mentioned that the hybrid combination composites showed more superior mechanical and corrosion properties over single reinforced composites. R. Beygi et al. [27] fabricated Al-TiC/Graphite hybrid composites using FSP with as-mixed Al-TiO₂-Gr powder mixture. They found a higher hardness and yield strength due to TiC (100 nm) produced in-situ for hybrid composites ball-milled mixture than that of as-mixed mixture.

It is generally agreed that Al alloy cannot exhibit sufficient strength against applications that involve rotating or reciprocating sliding contacts. Al alloys shows low sliding wear resistance when mated against several materials [28–32]. Amongst them, Al 7075 alloy is mainly used in structural applications of automobile and aerospace industry due to its high specific strength [33–35]. However, it has been observed that Al 7075 alloy possesses poor surface properties under various loading conditions. The fabrication of hybrid composites on Al alloys using FSP in order to improve their mechanical and tribological properties is found to be an effective method used by many researchers as discussed before. So far, attempts with the addition of hard SiC nano particles along with soft solid lubricant Gr nano particles reinforcement with Al 7075 as a base alloy using FSP, in order to improve its

tribological properties is not yet reported. Also, the response surface methodology (RSM) optimization of a FSP process including reinforcement's volume percentage, hybrid ratio, tool rotational speed and tool traverse speed as independent variables parameters to enhance surface properties Al alloys has not yet been reported. Thus, in this project the strategic attempt to improve Al 7075-T651 surface tribological properties by reinforcing SiC and Gr nano particles using the FSP technique is performed and discussed in detail. The optimization of the reinforcement hybrid ratio, volume percentage and FSP tool rotational and traverse speed is planned using RSM-designed experiments in order to improve the microhardness and wear properties of the base material.

2. Experimental Procedure

2.1. Materials and Properties

Aerospace-grade rolled Al 7075-T651 aluminium alloy samples with dimensions of (110 mm × 150 mm × 6.35 mm) were used as the base metal. The chemical composition of Al 7075-T651 is presented in the Table 1. The SiC nano powder of particle size between 200 nm–2 µm and graphite (Gr) flakes of width up to 2 µm with thickness <40 nm are used as reinforcements. The sizes of reinforcements are confirmed with scanning electron microscopy (SEM) imaging.

Table 1. Chemical composition of Al 7075-T651 alloy.

Component	Al	Zn	Mg	Cu	Fe	Si	Ti	Cr	Mn	Other
Weight%	87.1–91.4	5.1–6.1	2.1–2.9	1.2–2	0.5	0.4	0.2	0.18–0.28	0.3	0.15

2.2. Preparation of Reinforcement Hybrid Compositions and Deposition Method Materials and Properties

The reinforcement nano particles are mixed together using turbular mixer in order to obtain well mixed different hybrid ratios. For each hybrid ratio of reinforcements, the reinforcements are run for 5 h in the turbular mixer. The color of the mixture is found different than the SiC and Gr nano powders. The surface blind holes method is used for pre-placing nano particles on the base alloy plates. The schematic presentation of deposition method is illustrated in Figure 1. The holes of 2 mm diameter and 4 mm depth are produced on the base alloy using Vertical turret milling machine. The surface blind holes method is used for depositing the SiC/Gr. The intercavity spacing maintained are 2 mm, 4 mm and 6 mm in order to control the volume percentage of reinforcements into the base alloy.

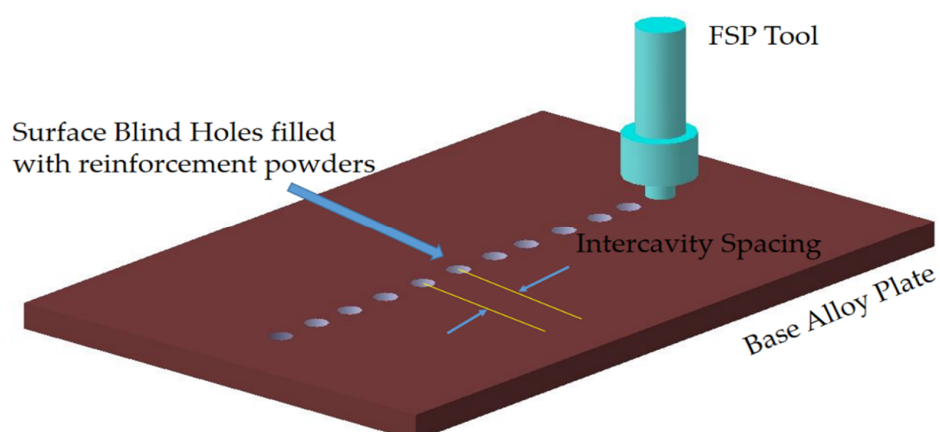


Figure 1. Surface blind holes deposition method.

The volume percentage of the SiC/Gr mixture into the base alloy is controlled by changing the number of blind holes on each band of the Al 7075 base alloy plate. The inter-cavity spacing was kept less than the diameter of the tool pin diameter to ensure continuous dispersion of SiC/Gr particles during the process, and thus to maintain continuity of the surface composites.

2.3. Friction Stir Processing and Testing Methodology

Initially, the reinforcement mixtures are put into the surface blind holes with proper compaction. Then capping process has been carried by using pinless H13 steel tool of 20 mm diameter. For all samples capping, the parameters used are: tool rotational speed of 1000 rpm and traversing speed of 30 mm/min, plunge depth of 0.3 mm, tool tilt angle (TT) of 2 degrees. The capping pass completely closes the surface cavities and traps the reinforcement particles inside. This ensures no reinforcement loss during the next FSP stirring action.

After completion of capping pass, single pass FSP on each sample has been carried out using a CHINA FSW CENTRE machine (Beijing FSW Technology Co., Ltd., Beijing, China). The H13 steel tool with straight cylindrical profile having 4.5 mm pin length, 6 mm pin diameter and 20 mm shoulder diameter is selected for FSP. During the FSP process, other parameters i.e., TT: 2 degrees, axial load-10 KN, and initial dwelling time:10 s have been kept constant for all samples. The optimum tool plunge depth of 5.3 mm is used for tool tilt angle of 2 degrees. With this tool plunge depth, the defects like tunnel and void have been successfully overcome. After prior preliminary tests, the limits of four independent parameters are decided and then using RSM optimization method in Design Expert 10 software, the experiments are designed. The designed experiments in central composite full factorial design module gives 27 runs as mentioned below in Table 2:

Table 2. Independent parameters and their levels for the designed experiments.

Parameter	Level -1	Level 0	Level 1
Tool Rotational Speed (w rpm)	500	1000	1500
Tool Traverse Speed (v mm/min)	20	30	40
Reinforcement Hybrid Ratio (HR)	60:40	75:25	90:10
Reinforcement Volume Percentage (Vol %)	4	8	12

The wear tests are conducted as per ASTM-G99 standards. The wear samples of size (L: 10 mm, W: 6 mm, T: 6 mm) are cut from the middle of each composite stir zone using wire EDM machine (Mitsubishi, Tokyo, Japan). These samples are used as pin in the pin-on disc arrangement. The discs of mild steel material are used in these tests. The pin-on-disc equipment used in these tests is Tribology Trainer Module TM 260 manufactured by Gunt Humburg. All 27 samples are tested and wear loss and coefficient of friction (COF) is measured as responses. The wear loss is measured as difference of weight difference of the wear samples before and after the test. The weight measurements are carried out using weight balance having least count of 0.1 mg. Each sample is run for 20 min at 150 rpm speed and under the loading of 20 N. The coefficient of friction of each sample is measured by taking the ratio of average craft force with the normal load.

The square-shaped samples of (20 mm × 20 mm) size cross-sectional were cut using wire electro-discharge machine. The specimen were mounted and polished with silicon carbide paper of increasing grit of 600, 800 and 1200. The sample was oriented 90° with each increment of silicon carbide paper. Further polishing of the sample was done by applying diamond slurry, 6 µm diamond paste and 3 µm diamond paste. Keller's reagent was used for etching with immersion time of 30 s and immediately clean with running water and dried. Field-emission scanning electron microscopy (FESEM, Phenom Pro X, Eindhoven, Netherlands) analysis was used to capture microscopic images within the SZ to study dispersion and interfaces between base alloy and reinforcements. Energy dispersive X-ray (EDX, Phenom Pro X, Eindhoven, Netherlands) and mapping facilities of FESEM equipment was used to further confirm and analyze the reinforcement's presence and dispersion within the stir zone.

The flash that has been formed during the FSP was removed by using diamond file to prevent misalignment of the specimen when the vision scope and indenter moves during Vickers microhardness (Leco LM 247AT, St. Joseph, MI, USA) testing. The specimen were tested with 1000 gf load with 15 seconds' dwell time. The indentation was measured on two diagonals (d1 and d2 in µm). 5 readings each were recorded on the stir zone (SZ) and the average value is utilized for further analysis.

3. Results and Discussion

3.1. Microstructural Characterization

In this study for microstructure analysis, the surface composites with highest (Run 24) and lowest (Run 10) wear rate (mg/m) have been cut and analysed. Figures 2 and 3 show FESEM micrographs containing distribution of SiC and Gr particles into the Al 7075 matrix for Run 10 and Run 24 composite stir zones. Figures 4 and 5 show the more magnified SEM micrographs of Al 7075-SiC/Gr composites of Run 10 and 24 samples showing the interfaces between base alloy and reinforcements. The presence of SiC and Gr particles and their dispersion was confirmed by FESEM energy dispersive X-ray (EDX) and mapping analysis as shown in Figures 6 and 7, respectively.

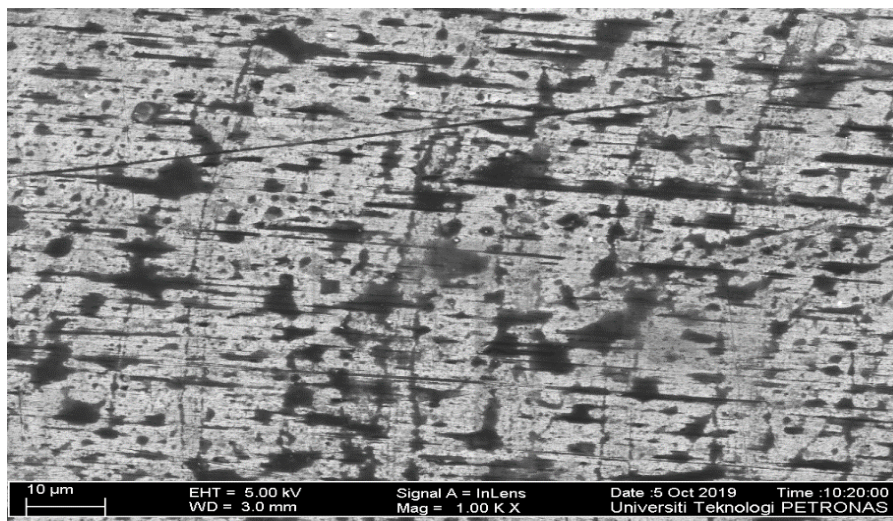


Figure 2. Field-emission scanning electron microscopy (FESEM) micrographs at magnification of 1000 × for Al 7075-SiC/Gr composite Run 10.

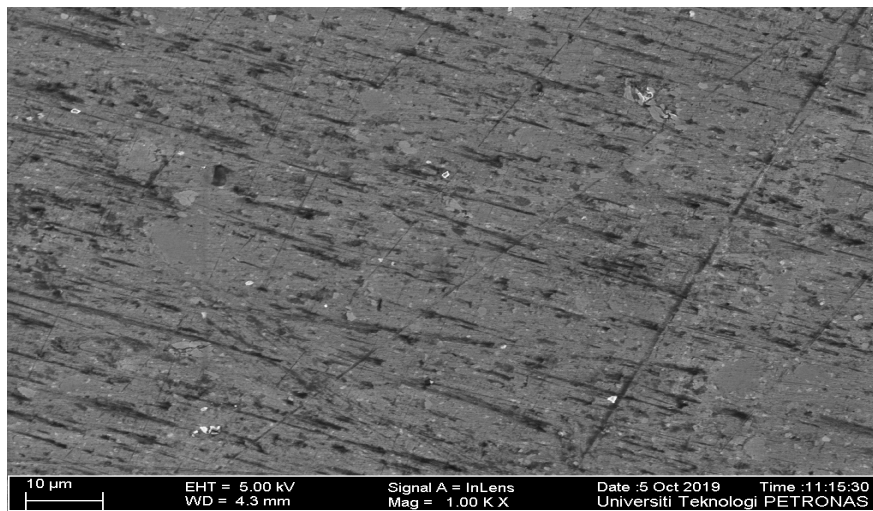


Figure 3. FESEM micrographs at magnification of 1000 × for Al 7075-SiC/Gr composite Run 24.

From Figure 4 micrographs of Run 10, it is observed that, the SiC particles are well surrounded by graphite flakes and the graphitized SiC particle zones are present in more numbers compared to Run 24 composite micrographs shown in Figure 5. In case of Run 10, due to very high rotational speed stirring action, the material movement has facilitated well dispersion of SiC/Gr powders and has given sufficient opportunity to encapsulate the graphitic layers around the SiC particles. The graphite flakes get exfoliated into multilayer graphene due to the shear action during intense

plasticization [24,25]. The graphite flakes have covered large area in the composites due to their large surface area. The SiC particles get fragmented in both samples have fragmented into uneven sizes due to the intense plasticization. The exfoliated graphitic layers have acted as a bridge between the SiC/Gr reinforcements and the base alloy, and has contributed for greater interfacial bonding. Due to very high thermal conductivity, the hybrid ratio of Gr is restricted to maximum 40%, as the high content of Gr than this limit has given tattering defects in the composite band [24].

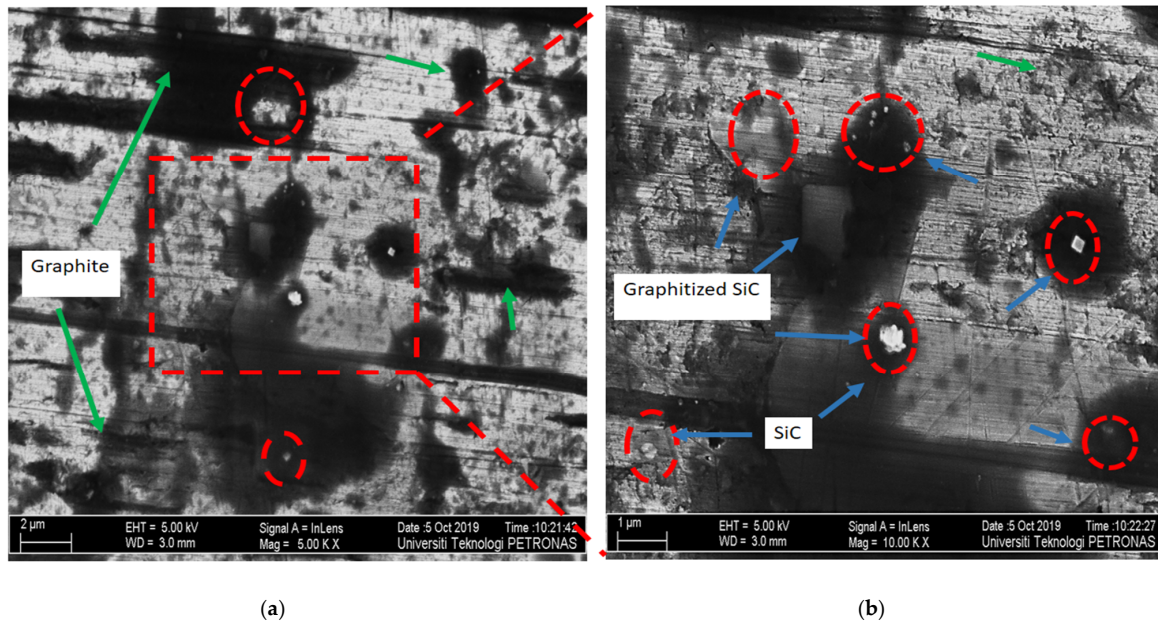


Figure 4. FESEM micrographs of Run 10-Al 7075-SiC/Gr composite with magnification of (a) 5 K \times and (b) 10 K \times .

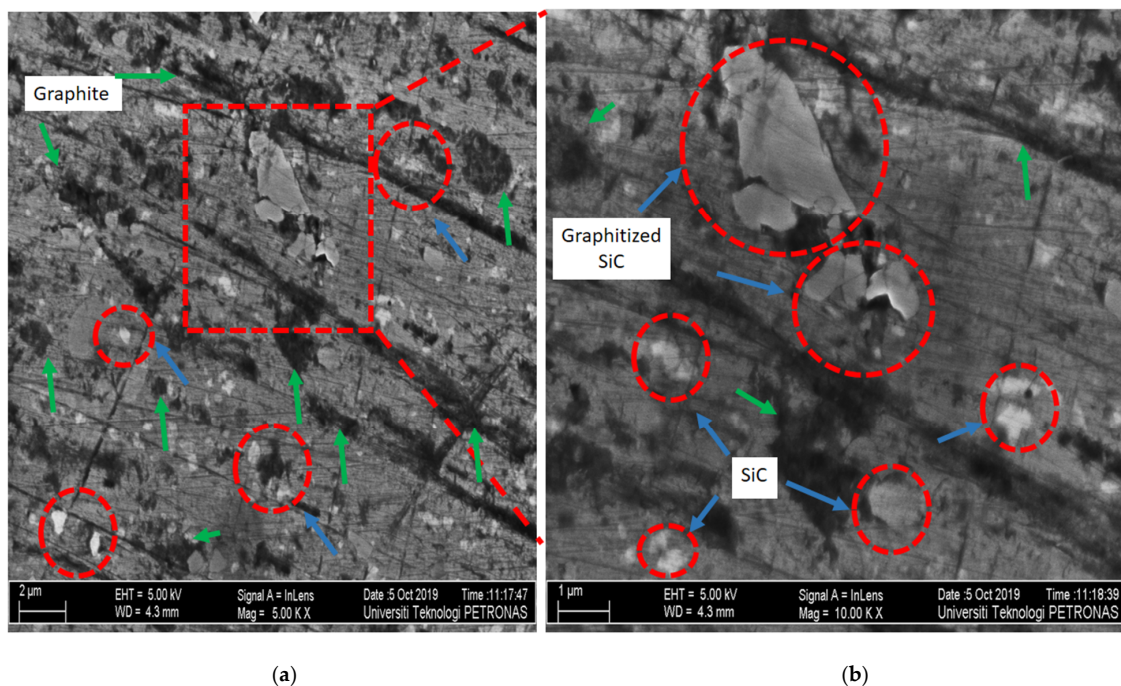


Figure 5. FESEM micrographs of Run 24-Al 7075-SiC/Gr composite (a) 5 K \times (b) 10 K \times .

The graphitized SiC particles in Run 10 are observed to have good interfacial bonding than the Run 24 composite sample. The extent of graphite layers encapsulating the SiC particles is more in case

of Run 10 sample than the Run 24 sample due to more intense stirring action. In both the samples, the hybrid ratio of 60:40 is used, but the intense plasticization due to high rotational speed in case of Run 10 has facilitated to overcome the flow stress of the base alloy prominently and thus the particles' interaction and mobilization inside the matrix have been increased. The greater volume percentage (12%) of SiC/Gr powder with lower rotational speed (500 rpm) in Run 24 has restricted the particle movement and dispersion during the stirring action. On the other hand, the low volume percentage of the SiC/Gr powder with high rotational speed (1500 rpm) has facilitated significant particle movement and dispersion in the matrix.

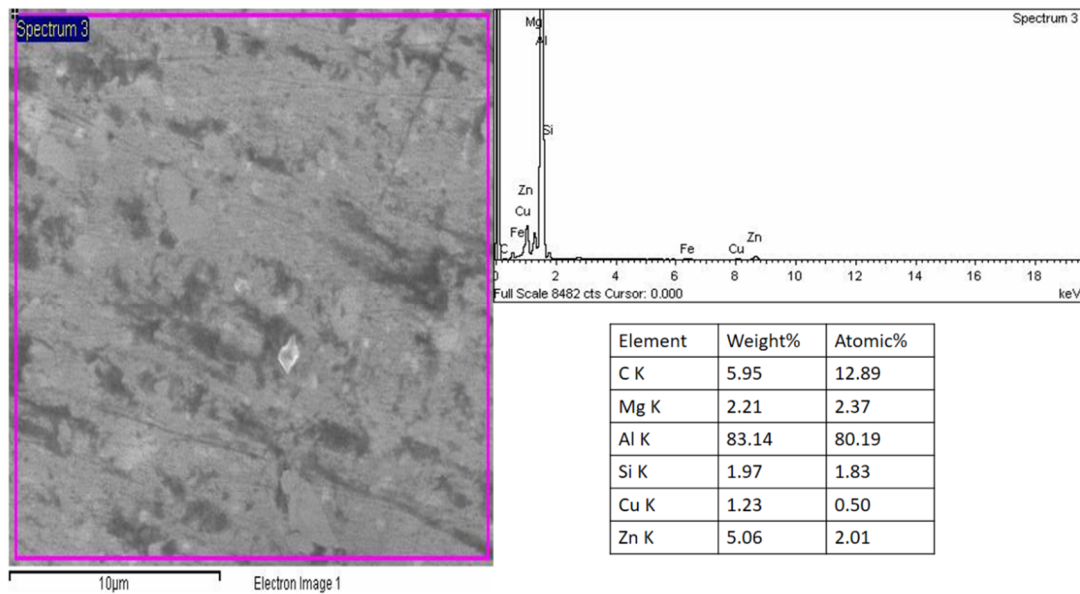


Figure 6. FESEM-energy-dispersive X-ray spectroscopy (EDX) analysis of Run 10-Al 7075-SiC/Gr composite.

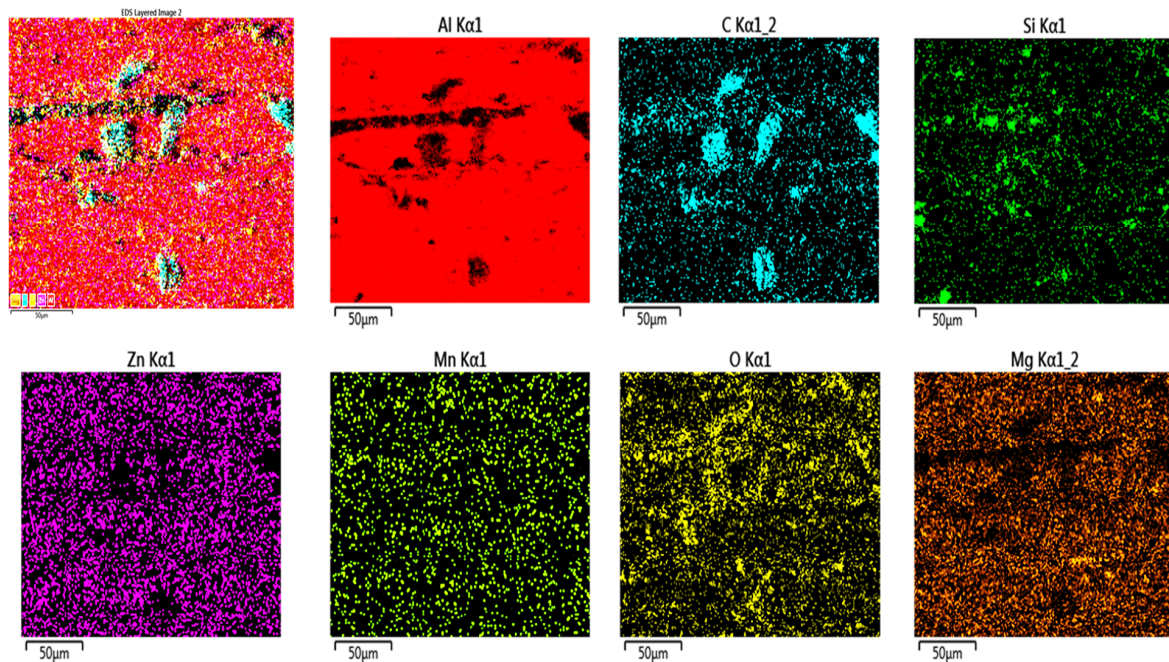


Figure 7. FESEM mapping analysis of Run 10-Al 7075-SiC/Gr composite.

The very thin graphite flakes have covered the more surface area inside the Al 7075-SiC/Gr composites as shown in Figure 7. Whereas the SiC particles have been fragmented and distributed

in the composites. The composite surfaces were different in appearance depending on the machine parameters and reinforcement dispersion. The SiC/Gr reinforcement particles dispersion inside the matrix has affected resultant grain size obtained inside the composites. The grain growth in processed composites is mainly controlled by the pinning effect due to presence of reinforcements. Thus due to encapsulation of reinforcements during intense plasticization the more refined grains structure is obtained in the resultant surface composites.

3.2. Wear Properties

The wear rate (mg/m) and average coefficient of friction for each sample has been measured and tabulated in Table 3. For all the Al 7075-SiC/Gr samples, the wear resistance has increased compared to the base alloy. Then wear rate as a response has been analyzed using analysis of variance (ANOVA). The ANOVA analysis results are given in Tables 4 and 5 below and the model for wear rate as a response is observed to be significant. The influence of independent variables with respect to wear rate are observed and discussed in below sections.

Table 3. Microhardness and wear properties of Al 7075-SiC/Gr hybrid surface composites.

Run	Tool Rotational Speed (W) rpm	Tool Traverse Speed (V) mm/min	Hybrid Ratio (HR)	Volume Percent (Vol %)	Wear Rate (mg/m)	Average Coefficient of Friction (COF)	Micro Hardness (HV)
1	500	20	90	12	0.03185	0.87	120.25
2	1500	20	90	12	0.03583	0.97	105.90
3	1500	20	60	12	0.04778	0.93	85.00
4	1000	30	90	8	0.01433	0.94	190.00
5	1000	20	75	8	0.03185	0.96	128.43
6	500	40	90	4	0.02627	0.87	118.65
7	500	20	90	4	0.02468	0.95	139.32
8	1500	30	75	8	0.01831	0.90	96.75
9	500	40	60	4	0.02707	0.92	116.83
10	1500	40	60	4	0.01194	0.91	114.5
11	500	40	90	12	0.02468	0.91	144.3
12	1000	30	75	8	0.01911	0.93	209.00
13	1500	40	90	12	0.03503	0.95	224.33
14	1000	30	75	12	0.02866	0.88	300.00
15	500	40	60	12	0.03583	0.97	233.8
16	1000	30	60	8	0.02389	0.98	189.24
17	1000	30	75	8	0.01991	0.93	185.0
18	1500	20	60	4	0.01672	0.93	91.4
19	500	20	60	4	0.03264	0.94	187.4
20	1500	40	90	4	0.02787	0.85	197.5
21	1000	30	75	8	0.01991	0.93	195.32
22	500	30	75	8	0.0239	0.87	132.3
23	1500	20	90	4	0.01592	0.97	128.35
24	500	20	60	12	0.05175	0.89	144.7
25	1500	40	60	12	0.03981	0.98	256.85
26	1000	40	75	8	0.02707	0.93	170.96
27	1000	30	75	4	0.01752	0.85	290.34

The contour diagram from Figures 8–10 show the ranges of four variables for the different intervals of wear rates of the hybrid surface composite samples. The minimum wear rate of 0.01194 mg/m is observed for Run 10 (w 1500 rpm, v 40 mm/min, HR 60:40, vol% 4) composite. Whereas highest wear rate of 0.05175 mg/m is obtained for Run 24 (w 500 rpm, v 20 mm/min, HR 60:40, vol% 12) composite specimen. The coefficient of friction values obtained varies between ranges of 0.85 to 0.98. From the ANOVA analysis, it has been observed that all four independent parameters are found significant.

Table 4. Analysis of variance (ANOVA) model validation of wear rate.

Source	Sum of Squares	df	Mean Square	F Value	p-Value Prob > F
Model	2.442×10^{-3}	14	1.744×10^{-4}	48.14	<0.0001
A	4.822×10^{-5}	1	4.822×10^{-5}	13.31	0.0033
B	6.216×10^{-5}	1	6.216×10^{-5}	17.15	0.0014
C	1.443×10^{-4}	1	1.443×10^{-4}	39.83	<0.0001
D	9.474×10^{-4}	1	9.474×10^{-4}	261.44	<0.0001
AB	4.055×10^{-5}	1	4.055×10^{-5}	11.19	0.0058
AC	9.125×10^{-5}	1	9.125×10^{-5}	25.18	0.0003
AD	1.726×10^{-4}	1	1.726×10^{-4}	47.63	<0.0001
BC	9.905×10^{-5}	1	9.905×10^{-5}	27.33	0.0002
BD	7.678×10^{-5}	1	7.678×10^{-5}	21.19	0.0006
CD	1.833×10^{-4}	1	1.833×10^{-4}	50.57	<0.0001
B ²	1.985×10^{-4}	1	1.985×10^{-4}	54.77	<0.0001
Residual	4.349×10^{-5}	12	3.624×10^{-6}		
Lack of Fit	4.306×10^{-5}	10	4.306×10^{-6}	20.18	0.0481
Pure Error	4.267×10^{-7}	2	2.133×10^{-7}		
Cor Total	2.486×10^{-3}	26			

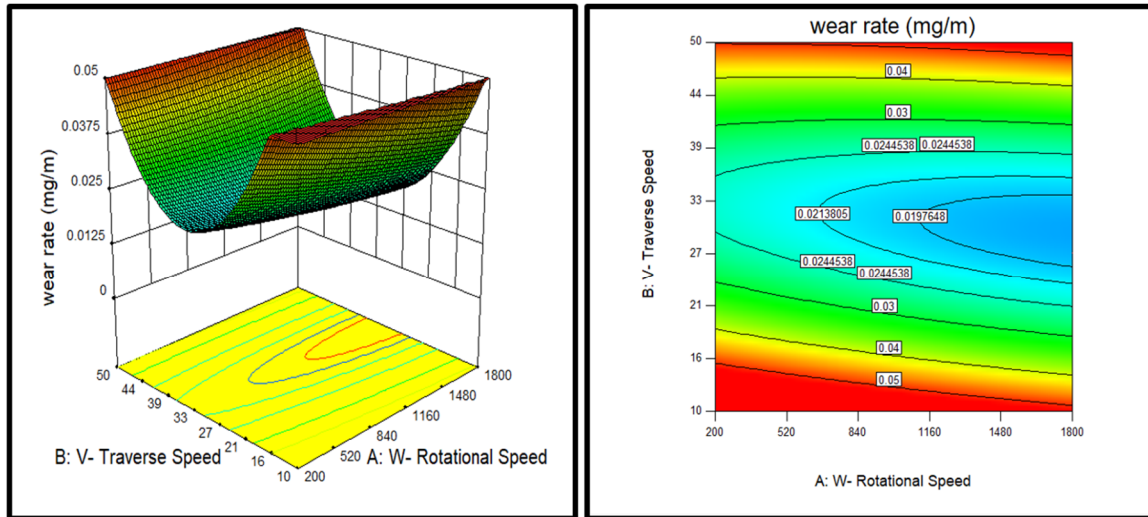
Table 5. Validation of model terms for wear rate.

Standard Deviation (Std. Dev.)	1.904×10^{-3}	R-Squared	0.9825
Mean	0.027	Adj R-Squared	0.9621
Coefficient of Variation (C.V.) %	7.04	Pred R-Squared	0.8866

From the analysis of plots of independent parameters against wear rate, the influence of each parameter on it is observed and important observations are as follows: (a) The desirable range of rotational speed is (1160–1500 rpm). The increase in tool rotational speed has shown decrease in wear rate due to more uniform distribution of SiC/Gr nano particles and thus results in strengthening of the composites by grain size strengthening and Orowan strengthening mechanism. The higher rotational speed facilitates the greater extent of intense plasticization, which provides more reinforcement movements. The Gr flakes exfoliated into multi-layered graphene and encapsulates around SiC particles and have contributed to more interfacial bonding. (b) the tool traverse speed has shown lower wear rates at the middle range 27–33 mm/min speeds. This is due to the effect of stirring action on reinforcement distribution and secondly on precipitations resizing and dispersion of the base alloy. The minimum traverse speed may have contributed to the heterogeneous distribution of reinforcements and agglomeration of powders will results into weak interfacial bonding and reinforcements piling out during wear tests. Therefore, in this study the traverse speed of around 30 mm/min has shown the minimum wear rate, at which balanced effect on distribution of reinforcement and precipitation dissolution would have occurred.

In the case of reinforcement related to two parameters, the effects are discussed as follows: (c) The hybrid ratio of SiC/Gr particles has shown effect on wear rate in such a way that the wear rate of the hybrid composites predicted minimum at the ranges in 50:50 to 60:40 ratios. The wear rate observed minimum at the Run 10 sample with HR of 60:40. The hard ceramic SiC particles will act as load-bearing elements and resists the wearing action due to their higher inherent hardness properties. On the other hand the Gr flakes on the surface of the wear tests samples has developed the mechanically mixed lubricating layer between the disc and pin. This Gr tribofilm once generated has reduced the wear rate due less friction and more gliding action during dry sliding actions. (d) Volume percentage of SiC/Gr reinforcement as a parameter has decided the desirable range for the optimum wear properties. From the analysis, it is predicted that the vol% between 3 and 6 will give lower wear rates. From the tests carried out, Run 10 with 4 vol% has shown minimum wear rate for the Al 7075-SiC/Gr surface composites. The volume percentage of reinforcements affects on grain size distribution, agglomeration

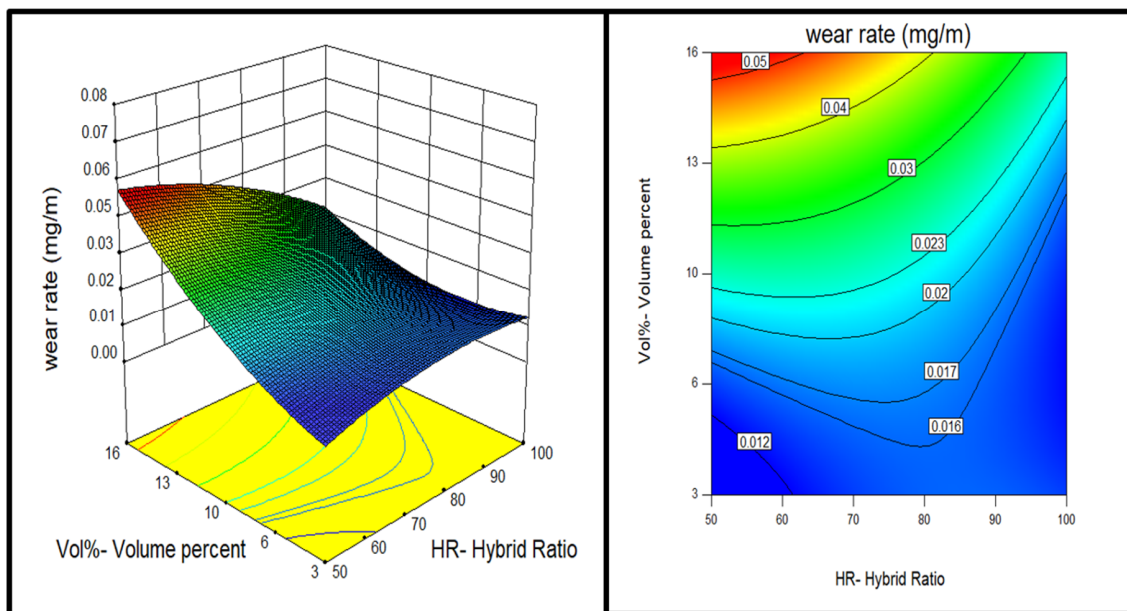
of powders, the required stirring action to overcome the flow stress of base alloy, finally the extent of interaction between reinforcements and interfacial bonding with the base alloy. The optimal amount of powder for the given stirring action has not only availed the homogenous distribution of reinforcements but also the significant strengthening by means of good interfacial bonding.



(a)

(b)

Figure 8. Influence of friction stir-processing (FSP) tool rotational and traverse speed on wear rate (a) 3D surface (b) contour plot.



(a)

(b)

Figure 9. Influence of FSP reinforcement hybrid ratio and volume percentage on wear rate (a) 3D surface (b) contour plot.

The wear tracks on the pins of base alloy, Run 10 composite and Run 24 composite are as shown in Figure 11. The clear difference is observed on the wear tracks of these materials, the composite's

surface morphology indicates presence of mechanically mixed tribo film over the surface in bright color due to reinforced SiC/Gr particles. The worn out surface of Al 7075 base alloy shows heterogeneous and adhesive wear mechanism, which is due to absence of any hard particles at the surface. Also, severe plastic deformations without any delamination, cracks of the base alloy indicate the adhesive wear mechanism. On the composite's worn out surfaces, the presence of hard graphitized SiC particles results in both abrasive and adhesive wear mechanism. Initially, due to adhesion, the wear loss occurred, further due to presence of graphitized SiC particles the resistance to wear increases and thus dimples, delaminations and cracks are observed on the surfaces.

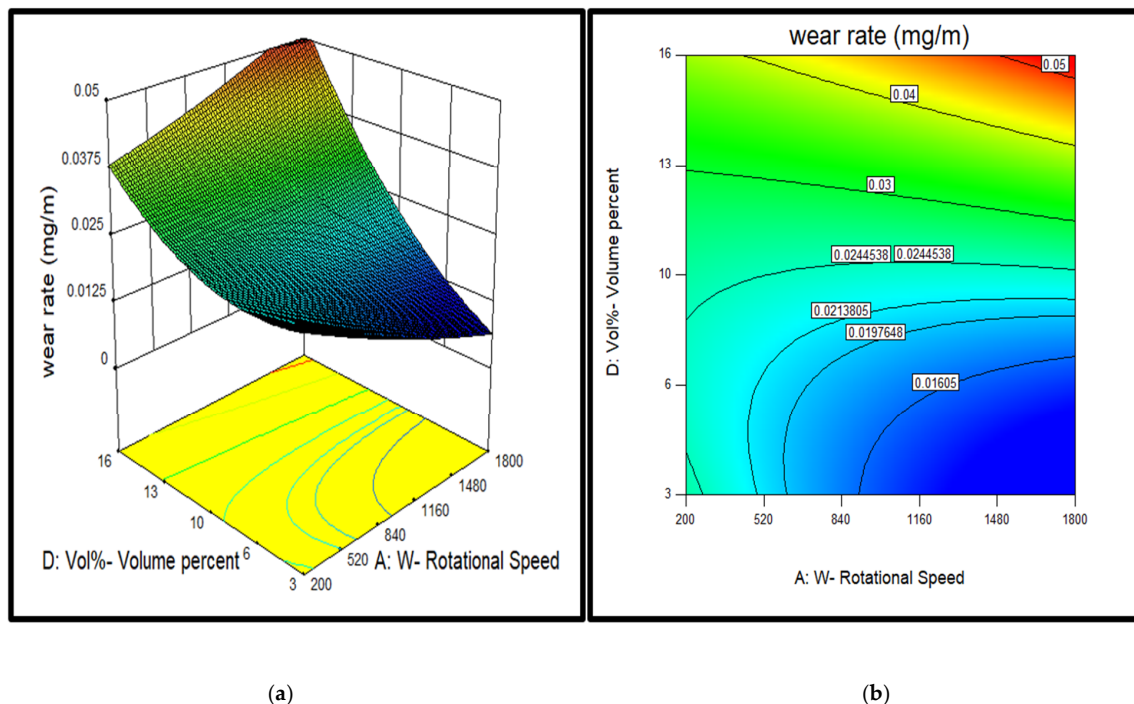


Figure 10. Influence of FSP tool rotational speed and reinforcement volume percentage on wear rate (a) 3D surface (b) contour plot.

Amongst the surface composites, the composites with high-volume percentage of reinforcements shows the pulling out of reinforcing particles due to loose interfacial bonding with the base alloy. The Run 24 wear track shows such particles pulling out due to agglomeration of powder and loose interfacial bonding with the base alloy, and thus resulted in higher wear rate. The wear mechanism has changed from adhesion to abrasion due to the presence of these hard reinforcement particle pulling out process. In case of Run 10 composite sample, the due to homogenous distribution and good interfacial bonding with the base alloy, the graphitized SiC reinforcement not only resists the wear prior to high hardness but also develops lubricative tribofilm due to graphitic flakes between mating surfaces. Thus, the wear rate was lower for Run 10 composite sample than the Run 24 sample.

The wear track of Run 10 composite has been analysed for confirming the presence of reinforcement SiC/Gr particles and mating steel disc particles. The FESEM-EDX analysis for such confirmation is shown in Figure 12 given below. The dark spots on the wear track confirms in terms of graphitized SiC particles as shown in spectrum 77 in the Figure 12. The highest carbon (C) presence confirms that those are the regions with SiC/Gr reinforcements.

The moderate dark uniform area confirms the presence of thin graphitic tribofilm since the spectrum 78 shows the C presence next to the base Al alloy as shown in Figure 12. Finally the spectrum 79 covers whole area of track under the scope and finalized prominent presence of SiC/Gr reinforcement and traces of steel disc particles as ferrous (Fe) element.

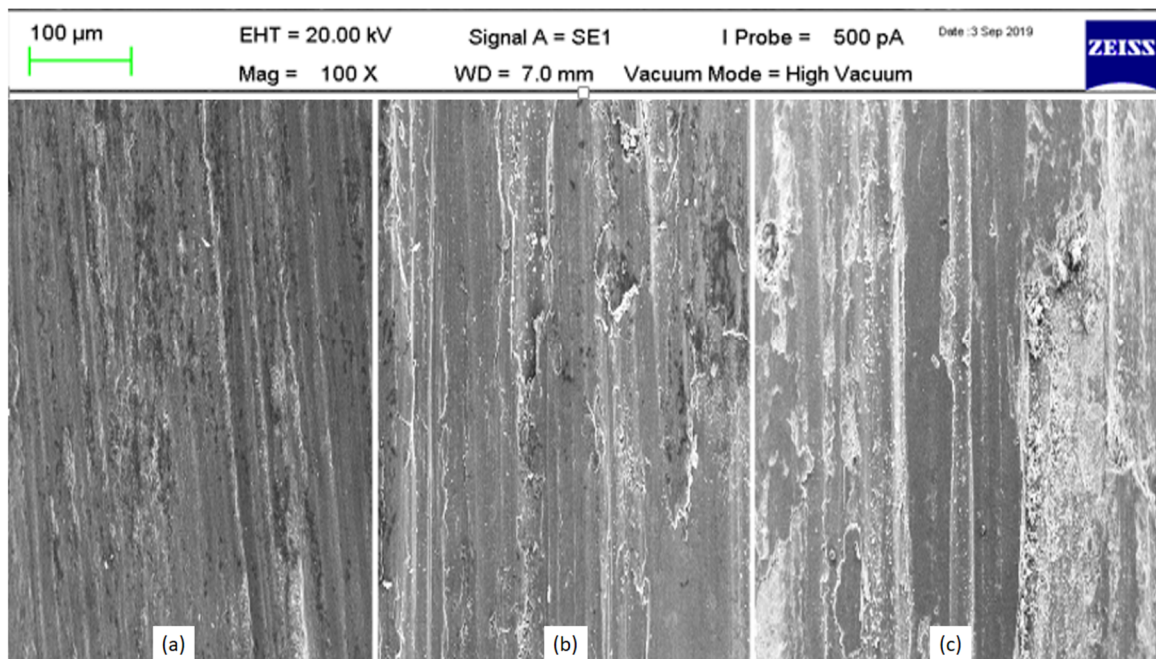


Figure 11. Wear tracks of (a) Base alloy, (b) Run 10 and (c) Run 24.

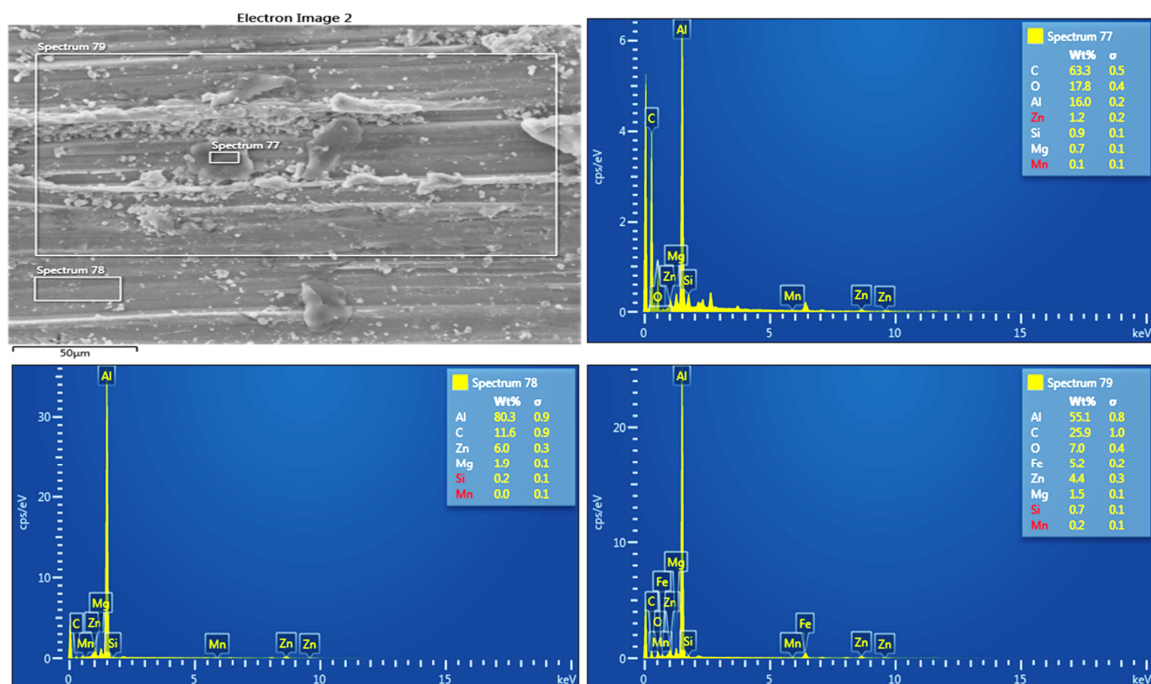


Figure 12. FESEM-EDX analysis on wear track of Run 10 Al 7075-SiC/Gr sample.

3.3. Microhardness

The Vickers’s microhardness tests are conducted on all the composite samples and the results are listed as shown in Table 3. The microhardness values are found some composites more and others less than the base alloy (140 HV). The base alloy used in this study is Al 7075-T651 and which has been heat treated. The FSP has contributed to the reduction of hardness for some composite samples due to dissolution of precipitates during highly intense super plastic deformation. Thus the ranges of tool rotational speed and tool traverse speed are important parameters deciding the extent of deformation. The maximum microhardness of 300 HV is found for Run 14 composite whereas minimum of 85 HV is

found for Run 3 surface composite. The increase in hardness is attributed to grain size strengthening due to restriction of grain growth by reinforcements pinning effects. So the microhardness has been mainly controlled in these composites by means of two mechanisms i.e., retaining of inherent precipitates within base alloy and uniform grain size strengthening due to the pinning effect. The increase in dislocation densities due to mismatch of thermal coefficients of reinforcements and base alloy also has contributed to enhancement in microhardness of resultant composites. Xiaofei Ju et al. [36] mentioned that the heat treatment (T6) on the FSPed composites retained the full precipitates solution in the base alloy along with same grain structure of composites. The ANOVA of microhardness as a response is given in Tables 6 and 7 below, the model is found to be significant.

Table 6. ANOVA analysis table of Microhardness.

Source	Sum of Squares	df	Mean Square	F Value	p-Value Prob > F
Model	86638.73	14	6188.48	17.57	< 0.0001
A	79.04	1	79.04	0.22	0.6442
B	11099.01	1	11099.01	31.51	0.0001
C	145.21	1	145.21	0.41	0.5329
D	2969.12	1	2969.12	8.43	0.0132
AB	8127.92	1	8127.92	23.08	0.0004
AC	4507.11	1	4507.11	12.80	0.0038
AD	221.12	1	221.12	0.63	0.4435
BC	31.70	1	31.70	0.090	0.7693
BD	10121.37	1	10121.37	28.74	0.0002
CD	2481.53	1	2481.53	7.05	0.0210
A ²	18500.13	1	18500.13	52.53	< 0.0001
B ²	6243.59	1	6243.59	17.73	0.0012
C ²	224.70	1	224.70	0.64	0.4400
D ²	23712.92	1	23712.92	67.33	< 0.0001
Residual	4226.40	12	352.20		
Lack of Fit	3935.73	10	393.57	2.71	0.2997
Pure Error	290.67	2	145.33		
Cor Total	90865.13	26			

Table 7. Validation of model terms of microhardness.

Standard Deviation (Std. Dev.)	18.77	R-Squared	0.9535
Mean	166.48	Adj R-Squared	0.8992
Coefficient of Variation (C.V.) %	11.27	Pred R-Squared	0.6583
PRESS	31052.22	Adeq Precision	16.083
-2 Log Likelihood	213.06	BIC	262.50
		AICc	286.70

The desirable ranges of independent parameters for maximizing the microhardness of composites is observed through following plots shown in Figures 13 and 14. From the plots it is confirmed that, for this heat treated base alloy both retaining of precipitations and grain size strengthening by more uniform reinforcements dispersion phenomenon are important in order to control the resultant microhardness. The retaining of precipitate solution depends on extent of stirring action. Thus high rotational speed at lower traverse speed has led to dissolution of precipitates solution. However, for same machine parameters condition, the SiC/Gr powder distribution will be high. In balancing conditions, the medium range of tool rotational speed (800–1120 rpm) and tool traverse speed around (30 mm/min) has given more microhardness properties for the resultant composites.

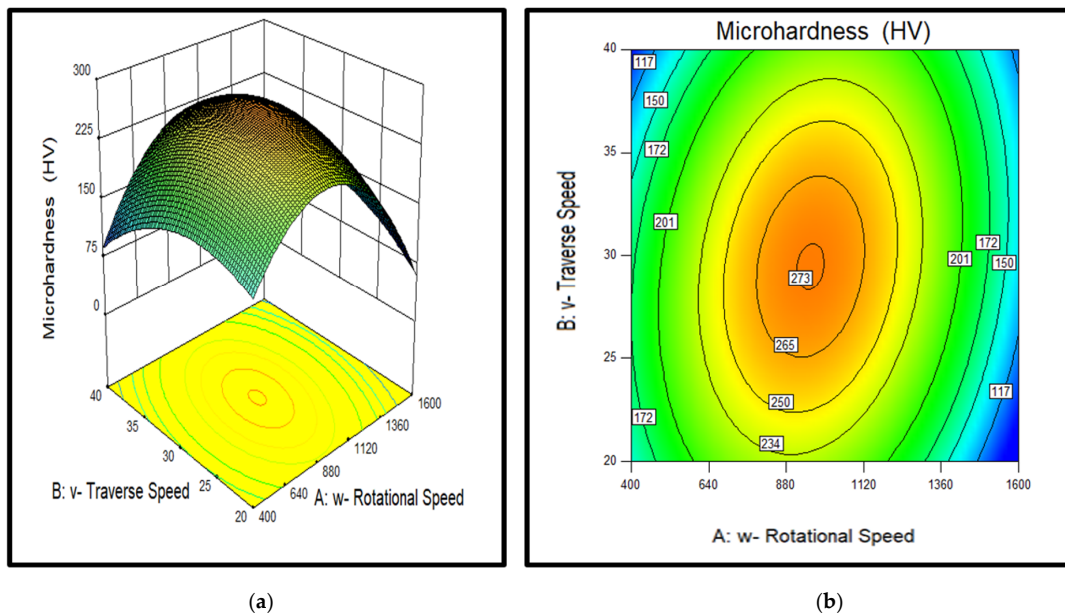


Figure 13. Influence of tool rotational speed and tool traverse speed on microhardness of Al 7075-SiC/Gr composites (a) 3D surface (b) contour plot.

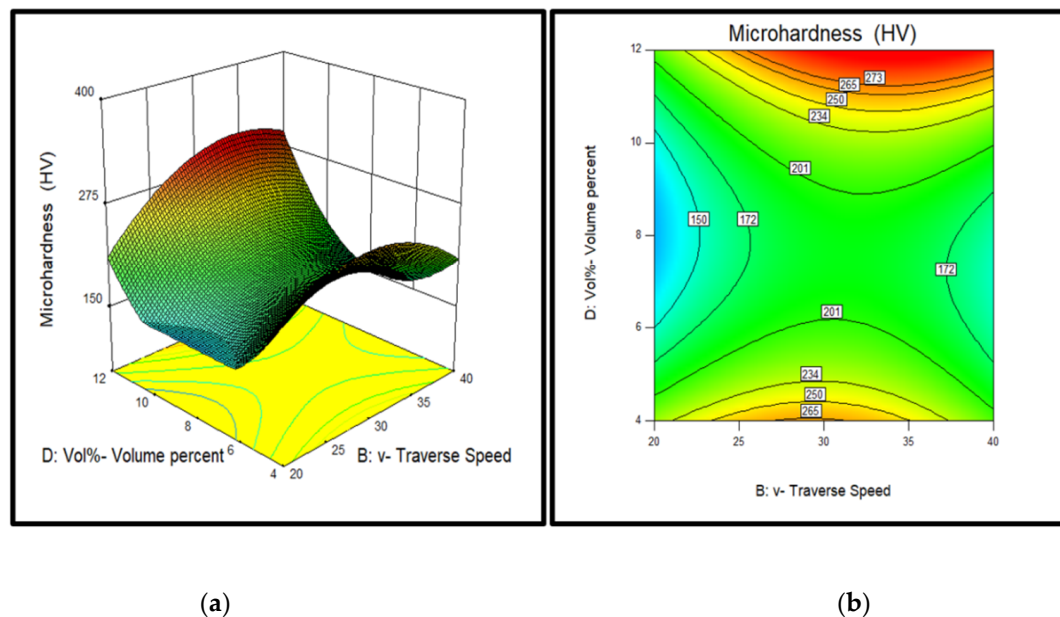


Figure 14. Influence of tool traverse speed and volume percentage on microhardness of Al 7075-SiC/Gr composites (a) 3D surface (b) contour plot.

In case of reinforcements volume percentage and hybrid ratio, it is observed from Figure 15 that the higher volume percentage (10–12%) and hybrid ratio between (60:40–70:30) has shown higher micro-hardness for the surface composites. Higher volume percentage of reinforcements have restricted grain growth in more extent due to which the more refined grain structure has to be obtained. The SiC particles are harder than the base alloy, so as its content increase resulted in higher microhardness of the composites. Although graphite flakes are softer than the base alloy, they have acted as a bridge between load-bearing SiC particles and base alloy to enhance the interfacial bonding. Thus these graphite exfoliation into multi layered graphene has supported in enhancing the microhardness of the resultant material.

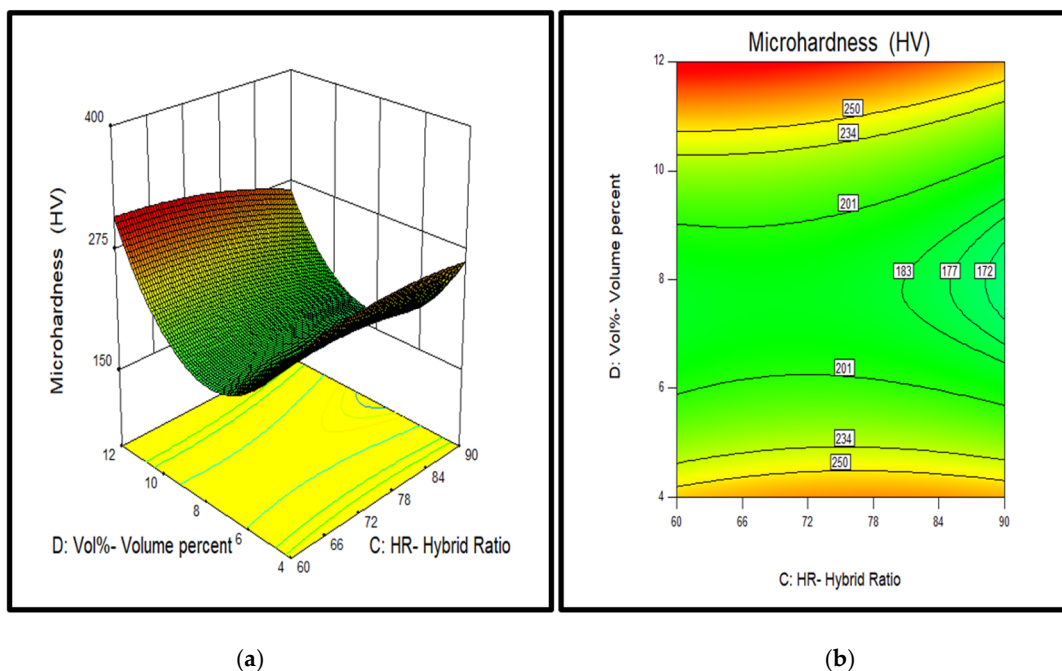


Figure 15. Influence of hybrid ratio and volume percentage on microhardness of Al 7075-SiC/Gr composites (a) 3D surface (b) contour plot.

Thus from the study, it is concluded that microhardness of Al 7075-SiC/Gr composites are controlled by all independent parameters in regard to their effect on resultant grain size distribution and retaining of inherent precipitates as mentioned in the above discussion.

4. Conclusions

The Al 7075-SiC/Gr hybrid surface composites are successfully fabricated using the FSP technique in the current work. Mainly, four FSP process parameters, i.e., tool rotational speed, tool traverse speed, reinforcement hybrid ratio and reinforcement volume percentage are optimized by performing designed experiments (DOE) using RSM central composite design (CCD) module in order to enhance microhardness and wear properties. The models for three responses, Microhardness, wear rate and coefficient of friction are found to be significant in the ANOVA analysis. The response variations are correlated with microstructural observations and important remarks are as given below:

- The optimum ranges of parameters observed for minimum wear rate are: w (1160–1500 rpm), v (27–33 mm/min), HR (50:50–60:40), vol% (3–6%).
- The optimal ranges of parameters observed for maximum microhardness are: w (800–1120 rpm), v (27–33 mm/min), HR (60:40–70:30) and vol% (10–12%).
- The wear rate has decreased significantly in Al 7075-SiC/Gr hybrid composites due to graphitized mechanically mixed tribofilm developed at the sliding contact zones.
- The wear rate increased due to powder agglomeration and the wear mechanism changed from adhesion to abrasion in the samples fabricated with low stirring action and high volume percentage of reinforcements.
- The microhardness of resultant composites observed to be dependent of effect of independent parameters on extent of precipitates dissolution and grain size strengthening in the resultant material. The enhancement in microhardness is attributed to the uniform dispersion of fragmented SiC along with exfoliated graphite layers which restricts the dislocation motion and induces grain size strengthening.

Author Contributions: The conceptualization of this research work is carried out by S.R.P. and N.A.P. The research work was carried out under the supervision of S.R.P. and O.B.M. The resources for the research were procured by S.R.P. The methodology, experiments, characterization and other tests were carried out by N.A.P. The tribological characterization was supervised by A.M.H.S.L. The original draft was written by N.A.P. The manuscript draft was reviewed by S.R.P. and O.B.M. The project administration and funding acquisition for this project was carried out by S.R.P.

Funding: This research received no external funding.

Acknowledgments: The work was supported by the Institute of Transport Infrastructure, Universiti Teknologi PETRONAS, Malaysia.

Conflicts of Interest: The authors declare no conflict of interest.

References

1. Dhanasekaran, S.; Sunilraj, S.; Ramya, G. SiC and Al₂O₃ reinforced aluminum metal matrix composites for heavy vehicle clutch applications. *Trans. Indian Inst. Met.* **2016**, *69*, 699–703. [[CrossRef](#)]
2. Bodunrin, M.O.; Alaneme, K.K. Aluminium matrix hybrid composites: A review of reinforcement philosophies mechanical corrosion and tribological characteristics. *J. Mater. Res. Technol.* **2015**, *4*, 434–445. [[CrossRef](#)]
3. Maurya, M.; Kumar, S.; Bajpai, V. Assessment of the mechanical properties of aluminium metal matrix composite: A review. *J. Reinf. Plast. Compos.* **2018**, *38*, 267–298. [[CrossRef](#)]
4. Li, K.; Liu, X.; Zhao, Y. Research Status and Prospect of Friction Stir Processing Technology. *Coatings* **2019**, *9*, 129. [[CrossRef](#)]
5. Gui, M.; Kang, S.B.; Euh, K. Influence of spraying conditions on microstructures of Al-SiC p composites by plasma spraying. *Metall. Mater. Trans.* **2005**, *36*, 24–71. [[CrossRef](#)]
6. Bakshi, S.R.; Singh, V.; Balani, K.; McCartney, D.G. Carbon nanotube reinforced aluminum composite coating via cold spraying. *Surf. Coat. Technol.* **2008**, *202*, 51–62. [[CrossRef](#)]
7. Hu, C.; Xin, H.; Baker, T.N. A new aluminium silicon carbide formed in laser processing. *J. Mater. Sci.* **1997**, *32*, 5047. [[CrossRef](#)]
8. Pantelis, D.; Tissandier, A.; Manolatos, P.; Ponthiaux, P. Formation of wear resistant Al-SiC surface composite by laser melt-particle injection process. *Mater. Sci. Technol.* **1995**, *11*, 299–303. [[CrossRef](#)]
9. Hu, C.; Xin, H.; Baker, T.N. Laser processing of an aluminium AA6061 alloy involving injection of SiC particulate. *J. Mater. Sci.* **1995**, *32*, 5047–5051. [[CrossRef](#)]
10. Katipelli, L.R.; Dahotre, N.B. Mechanism of high temperature oxidation of laser surface engineered TiC/Al alloy composite coating on 6061 aluminium alloy. *Mater. Sci. Technol.* **2001**, *17*, 1061–1068. [[CrossRef](#)]
11. Wang, Y.; Zhang, X.; Zeng, G.; Li, F. In situ production of Fe-VC and Fe-TiC surface composites by cast-sintering. *Composites Part A.* **2001**, *32*, 281–286. [[CrossRef](#)]
12. Wang, Y.; Zhang, X.; Zeng, G.; Li, F. Cast sinter technique for producing iron base surface composites. *Mater. Des.* **2000**, *21*, 447–452. [[CrossRef](#)]
13. Nagabhyrava, R.; Kota, S.; Geda, A.; Gudi, S.H. Investigation of mechanical properties of Al 7075/SiC/Gr hybrid metal matrix composites. *IJMET* **2017**, *8*, 265–269.
14. Khodabakhshi, F.; Simchi, A. The role of microstructural features on the electrical resistivity and mechanical properties of powder metallurgy Al-SiC-Al₂O₃ nano composites. *Mater. Des.* **2017**, *130*, 26–36. [[CrossRef](#)]
15. Wang, Q.; Zhang, B.; Ren, Y.; Yang, K. Eliminating detrimental effect of cold working on pitting corrosion resistance in high nitrogen austenitic stainless steels. *Corros. Sci.* **2017**, *123*, 351–355. [[CrossRef](#)]
16. Gangil, N.; Siddiquee, N.; Maheshwari, S.; Abdulrahman, M.A.; Abidi, M.H. State of the art of ex-situ aluminium matrix composite fabrication through friction stir processing. *Arch. Metall. Mater.* **2018**, *63-2*, 719–738.
17. Gangil, N.; Siddiquee, A.N.; Maheshwari, S. Aluminium based in-situ composite fabrication through friction stir processing: A review. *J. Alloys Compd.* **2017**, *715*, 91–104. [[CrossRef](#)]
18. Mishra, R.S.; Ma, Z.Y.; Charit, I. Friction stir processing: A novel technique for fabrication of surface composite. *Mater. Sci. Eng.* **2003**, *341*, 307–310. [[CrossRef](#)]
19. Khan, N.Z.; Siddiquee, A.N.; Khan, Z.A.; Mukhopadhyay, A.K. Mechanical and microstructural behavior of friction stir welded similar and dissimilar sheets of AA2219 and AA7475 aluminium alloys. *J. Alloys Compd.* **2017**, *695*, 2902–2908. [[CrossRef](#)]

20. Mathers, G. *The Welding of Aluminium and Its Alloys*, 1st Ed. ed; Woodhead Publishing Limited: England, UK, 2002.
21. Mandal, N.R. *Aluminium Welding*; Woodhead Publishing Limited: Cambridge, UK, 2002.
22. Dong, H. *Surface Engineering of Light Alloys Aluminium, Magnesium and Titanium Alloys*; Wood head Publications: England, UK, 2010.
23. Singh, J.; Chauhan, A. A review on dry sliding wear behavior of Al composites for automotive applications. *Tribol. Online.* **2014**, *9*, 121–134. [[CrossRef](#)]
24. Dixit, S.; Mahata, A.; Mahapatra, D.R.; Kailas, S.V.; Chattopadhyay, K. Multi-layer graphene reinforced aluminum—Manufacturing of high strength composite by friction stir alloying. *Composites Part B* **2018**, *136*, 63–71. [[CrossRef](#)]
25. Singh, S.; Rathi, K.; Pal, K. Synthesis, characterization of graphene oxide wrapped silicon carbide for excellent mechanical and damping performance for aerospace application. *J. Alloys Compd.* **2018**. [[CrossRef](#)]
26. Sharma, A.; Sharma, V.M.; Sahoo, B.; Jomy, J.; Paul, J. Effect of exfoliated few-layered graphene on corrosion and mechanical behaviour of the graphitized Al–SiC surface composite fabricated by FSP. *J. Bull. Mater. Sci.* **2019**, *42*, 204. [[CrossRef](#)]
27. Beygi, R.; Mehrizi, M.Z.; Eisaabadi, G.B. Friction Stir Processing of Al with Mechanically Alloyed Al-TiO₂-Graphite Powder: Microstructure and Mechanical Properties. *J. Mater. Eng. Perform. ASM Int.* **2017**, *26*, 3–1455. [[CrossRef](#)]
28. Zalensas, D.L. *Aluminum Casting Technology*, 2nd ed.; American Foundry Society: Schaumburg, IL, USA; University of Virginia: Charlottesville, VA, USA, 1997.
29. Sahin, Y. Wear behaviour of aluminium alloy and its composites reinforced by SiC particles using statistical analysis. *Mater. Des.* **2003**, *24*, 95–103. [[CrossRef](#)]
30. Kumar, R.; Dhiman, S. A study of sliding wear behaviors of Al-7075 alloy and Al-7075 hybrid composite by response surface methodology analysis. *Mater. Des.* **2013**, *50*, 351–359. [[CrossRef](#)]
31. Gravier, N.P.; Cutiongco, E.C.; Chung, Y.W. Effect of testing environments on friction and bidirectional material transfer during dry sliding of 3004-aluminum against H13 steel. *Tribol. Trans.* **1995**, *38*, 168–172. [[CrossRef](#)]
32. Zhang, J.; Alpas, A.T. Wear regimes and transitions in Al₂O₃ particulate reinforced aluminum alloys. *Mater. Sci. Eng. A* **1993**, *161*, 273–284. [[CrossRef](#)]
33. Rajan, R.; Kah, P.; Mvola, B.; Martikainen, J. Trends in Aluminium Alloy Development and their Joining Methods. *Rev. Adv. Mater. Sci.* **2016**, *44*, 383–397.
34. Dursun, T.; Soutis, C. Recent developments in advanced aircraft aluminium alloys. *Mater. Des.* **2014**, *56*, 862–871. [[CrossRef](#)]
35. Rambabu, P.; Prasad, N.E.; Kutumbarao, V.V.; Wanhill, R.J.H. *Aluminium Alloys for Aerospace Applications*; Springer Science, Business Media Singapore: Singapore, 2017.
36. Ju, X.; Zhang, F.; Chen, Z.; Ji, G.; Wang, M.; Wu, Y.; Zhong, S.; Wang, H. Microstructure of Multi-Pass Friction-Stir-Processed Al-Zn-Mg-Cu Alloys Reinforce by Nano-Sized TiB₂ Particles and the Effect of T6 Heat Treatment. *Metals* **2017**, *7*, 530. [[CrossRef](#)]



© 2019 by the authors. Licensee MDPI, Basel, Switzerland. This article is an open access article distributed under the terms and conditions of the Creative Commons Attribution (CC BY) license (<http://creativecommons.org/licenses/by/4.0/>).